

RL-MILP Solver: A Reinforcement Learning Approach for Solving Mixed-Integer Linear Programs with Graph Neural Networks

Tae-Hoon Lee¹ Min-Soo Kim¹

Abstract

Mixed-integer linear programming (MILP) is a widely used optimization technique across various fields. Existing *end-to-end learning* methods for MILP generate values for a subset of decision variables and delegate the remaining problem to traditional MILP solvers. However, this approach often fails to guarantee solution feasibility (i.e., satisfying all constraints) due to inaccurate predictions and primarily focuses on binary decision variables. Satisfying all constraints is a prerequisite for obtaining the optimal solution, and the feasibility issue becomes even more critical with non-binary integer (integer, for short) variables. Thus, addressing the feasibility of MILP involving integer variables is crucial. To address these challenges, we propose a novel reinforcement learning (RL)-based solver that not only finds the first feasible solution but also incrementally discovers better feasible solutions without delegating the remainder to off-the-shelf solvers. Our experimental results demonstrate that the proposed method achieves (near-)optimal solutions.

1. Introduction

The traveling salesman problem and the knapsack problem are classic examples of combinatorial optimization (CO) problems, extensively studied in operations research and computer science (Gasse et al., 2022). CO involves mathematical optimization that aims to minimize or maximize a specific objective function (Mazyavkina et al., 2021). If the objective function and constraints of CO are linear, it is called linear programming (LP). Furthermore, if some variables in LP must take integer values, it becomes Mixed-integer linear programming (MILP) (Bengio et al., 2021). MILP is widely applied to real-world scenarios such as logistics (Kweon et al., 2024) and path planning (Zuo et al., 2020).

¹School of Computing, Korea Advanced Institute of Science and Technology, Daejeon, Republic of Korea.
Corresponding author: Min-Soo Kim <minsoo.k@kaist.ac.kr>.

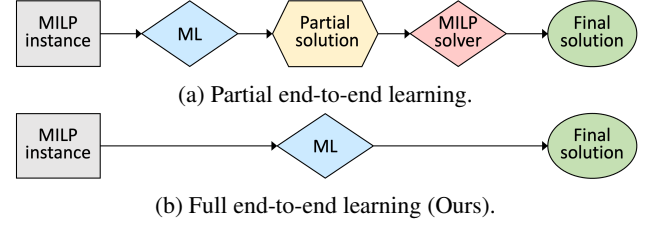


Figure 1: Solving MILP with *end-to-end learning* methods.

ML methods that directly learn and generate solutions for CO problems are categorized as an *end-to-end learning* approach (Bengio et al., 2021). ML-based primal heuristics are considered as *end-to-end learning* (Han et al., 2023), which aim to quickly find solutions to MILP by reducing the search space (Achterberg et al., 2012). Unlike traditional primal heuristics, which rely on expert knowledge and hand-crafted designs (Bengio et al., 2021), the ML-based one leverages similar patterns shared by MILP instances generated from a specific distribution (Gasse et al., 2022). Figure 1(a) illustrates how ML-based primal heuristics solve MILP. A trained ML model generates a partial solution for a subset of integer variables, which is then passed to a traditional solver (e.g., Gurobi and SCIP) to optimize the remaining sub-problem, referred to as partial end-to-end learning.

Existing ML-based primal heuristics have demonstrated their ability to quickly find good solutions (Gasse et al., 2019; Nair et al., 2020; Yoon, 2022; Han et al., 2023; Cantürk et al., 2024). However, inaccurate ML predictions hinder solution feasibility, which emphasizes the importance of feasibility (Han et al., 2023). The infeasibility obstructs reaching the optimal solution, posing a significant obstacle to solving MILP. Moreover, the existing studies mostly focus on the prediction for binary decision variables. However, many real-world problems involve non-binary integer (integer, for short) variables such as logistics (Kweon et al., 2024), maritime transportation (Papageorgiou et al., 2014), and energy systems (Ren & Gao, 2010). This highlights the need for techniques that can handle integer variables.

Infeasibility caused by incorrect ML predictions can be more pronounced for integer variables due to their broader range than binary variables. Imagine a naïve ML approach

that predicts the value of an integer variable x_i whose range is $[0, 1000]$. The maximum possible prediction error for x_i would be larger than binary variables because the range of x_i is broader than binary variables whose range is $[0, 1]$. Moreover, rounding predicted values to integers may cause additional accuracy loss (Cont & Heidari, 2014). A method for handling integer variables in partial end-to-end learning has been proposed, representing values in binary format. (Nair et al., 2020). In binary format, x_i has the sequence length of $\lceil \log_2(1000) \rceil = 10$, requiring multiple dimensions for a single variable. Even in some cases, the upper/lower bounds of variables are infinite, as seen in the default setting in SOTA solver, Gurobi Optimization. Thus, it calls for a more sophisticated and scalable approach (Cantürk et al., 2024).

To address this, we propose a RL-based method for solving MILP, called RL-MILP solver. Figure 1(b) illustrates how our solver derives the final solution. Unlike the partial end-to-end learning methods that focus on a subset of binary variables, the RL-MILP solver generates complete feasible solutions for MILP involving integer variables without delegating the sub-problem to traditional solvers. Moreover, as a RL-based method, the RL-MILP solver does not require the labeled data in contrast to those methods. As an initial study on full end-to-end RL-based MILP solvers, our study opens the door to a unified LP solver for multiple CO tasks, which is desirable in real-world scenarios (Liu et al., 2024).

We design a RL system tailored to MILP, which enables the agent to learn the variable-constraint relationships. Our method decides whether to change the value of integer variables rather than directly predicting their exact values. The solution search process is divided into two phases: before and after finding the first feasible solution. We design a reward function to align with the objectives of each phase. The RL agent is trained based on the degree of constraint violations and the solution quality. We adopt a Transformer-based GNN to capture relationships among distant variables. The agent improves the solution quality guided by the proposed search strategy. Experimental results demonstrate that the RL-MILP solver achieves optimal solutions on a small dataset and finds near-optimal solutions under a 1% gap for larger datasets. Our main contributions are as follows:

- We propose a novel RL-MILP solver that incrementally improve feasible solutions for MILP involving integer variables without reliance on off-the-shelf solvers.
- We design a RL system that enables the agent to learn problem-solving capabilities by learning relationships between decision variables and constraints.
- We propose learning and search strategies for solving MILP problems grounded in a theoretical foundation.
- We propose a Transformer-based GNN as the agent’s architecture, designed to effectively capture the complex relationships among decision variables.

2. Preliminaries

2.1. Mixed-Integer Linear Programming

2.1.1. A STANDARD FORM

Mixed-integer linear programming (MILP) is an optimization problem that minimizes or maximizes a linear objective function while satisfying linear constraints and integrality requirements for some decision variables (Bertsimas & Tsitsiklis, 1997). A standard form of MILP is as follows:

$$\text{minimize } \mathbf{c}^T \mathbf{x} \quad (1)$$

$$\text{subject to } \mathbf{A} \mathbf{x} \leq \mathbf{b} \quad (2)$$

$$x_i \in \mathbb{Z}, \forall i \in I \quad (3)$$

$$l_i \leq x_i \leq u_i, \forall i \quad (4)$$

where $\mathbf{x} \in \mathbb{R}^n$ is a column vector of n decision variables, $\mathbf{c} \in \mathbb{R}^n$ is a column vector of the objective coefficients, $\mathbf{A} \in \mathbb{R}^{m \times n}$ is the constraint coefficient matrix, $\mathbf{b} \in \mathbb{R}^m$ is a column vector of the right-hand side of the constraints, I is the index set of integer decision variables, l_i/u_i denotes the lower/upper bounds for each decision variable x_i . The goal of MILP is to find the optimal solution, and for a minimization problem, this corresponds to a feasible solution \mathbf{x} that minimizes $obj = \mathbf{c}^T \mathbf{x}$ (Eq. 1). A feasible solution is a solution \mathbf{x} that satisfies all constraints (Eqs. 2-4).

All MILP problems can be transformed into the standard form (Eqs. 1-4) (Bertsimas & Tsitsiklis, 1997). Let \mathbf{a}_i^T denote a row vector of a single constraint, $\mathbf{A} = (\mathbf{a}_1^T, \dots, \mathbf{a}_m^T)$, and $\mathbf{b} = (b_1, \dots, b_m)$. An equality constraint $\mathbf{a}_i^T \mathbf{x} = b_i$ is equivalent to two inequality constraints ($\mathbf{a}_i^T \mathbf{x} \geq b_i$ and $\mathbf{a}_i^T \mathbf{x} \leq b_i$). Moreover, $\mathbf{a}_i^T \mathbf{x} \geq b_i$ is equivalent to $-\mathbf{a}_i^T \mathbf{x} \leq -b_i$. Similarly, maximizing $\mathbf{c}^T \mathbf{x}$ is equivalent to minimizing $-\mathbf{c}^T \mathbf{x}$. Regardless of the direction of the objective function or constraints, a problem can be reformulated in the standard form. Thus, we only address standard-form problems (i.e., minimization) in the following sections.

2.1.2. KEY PROPERTIES OF MILP

MILP is known to be NP-hard, with integrality requirements (Eq. 3) (Nair et al., 2020). As the number of integer variables increases, its computation cost grows exponentially (Floudas, 1995). LP-relaxation refers to the technique of removing the integrality requirement, which transforms an original MILP problem into an LP problem solvable in polynomial time (Bertsimas & Tsitsiklis, 1997). LP-relaxation is commonly used to obtain an initial solution and a lower bound for the original problem (Witzig et al., 2021) as such in traditional algorithms (e.g., Branch-and-Bound (Land & Doig, 2010) and Feasible Pump (Fischetti et al., 2005)). Letting obj_r be the optimal value of the LP-relaxed problem and obj_b be the objective value obtained by the current best feasible solution of the given original MILP problem, Proposition 1 is derived as follows:

Proposition 1. *If a better feasible solution \mathbf{x}' exists for a given MILP problem, \mathbf{x}' must yield obj' that lies between obj_r and obj_b .*

The proof of Proposition 1 is provided in Appendix A. Drawing on Proposition 1, we design our RL system to guide exploration toward the optimal solution.

2.2. Graph for MILP and Graph Neural Networks

2.2.1. BIPARTITE GRAPH REPRESENTATION OF MILP

Studies on ML-based primal heuristics represent MILP instances as bipartite graphs (Gasse et al., 2019; Nair et al., 2020; Yoon, 2022; Han et al., 2023; Cantürk et al., 2024). In a bipartite graph representation of MILP, one set of nodes is for constraints, and the other is for decision variables. An edge connects a variable node to a constraint node only if the variable appears in the corresponding constraint. For example, in Figure 2(a), the variable x_3 appears in the constraint \mathbf{a}_2 . Therefore, in the MILP bipartite graph, the variable node for x_3 is connected to the constraint node for \mathbf{a}_2 .

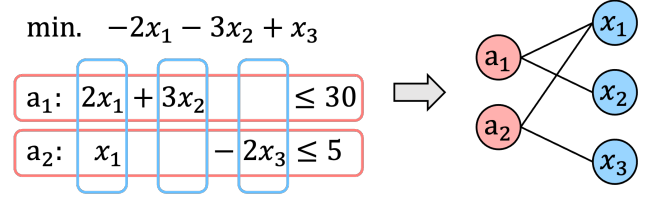
2.2.2. MESSAGE PASSING NEURAL NETWORK

The message passing neural network (MPNN) (Gilmer et al., 2017) is a general framework for message passing-based GNNs. Widely used GNNs such as GCN (Kipf & Welling, 2017), GAT (Veličković et al., 2018), and GIN (Xu et al., 2019) are the architectures based on MPNN. Given a graph G , the new representation $h_v^{(k+1)}$ is obtained as follows:

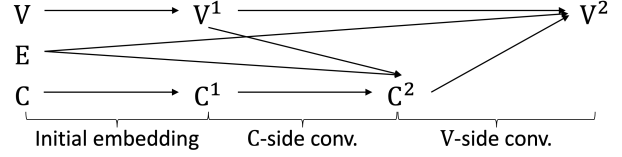
$$\begin{aligned} m_{vu}^{(k+1)} &= msg(h_v^{(k)}, h_u^{(k)}, e_{vu}), \forall e_{vu} \in \mathcal{E} \\ g_v^{(k+1)} &= agg(\{m_{vu}^{(k+1)} | u \in \mathcal{N}(v)\}), \forall v \in \mathcal{V} \\ h_v^{(k+1)} &= update(h_v^{(k)}, g_v^{(k+1)}), \forall v \in \mathcal{V} \end{aligned} \quad (5)$$

where $h_v^{(0)}$ is the initial feature vector of a target node v , and $msg(\cdot)$, $agg(\cdot)$, and $update(\cdot)$ are the message-passing, aggregation, and update functions, respectively. $msg(\cdot)$ generates a message $m_{vu}^{(k+1)}$ using the representation of the target node $h_v^{(k)}$, the neighbor node $h_u^{(k)}$, and the edge feature e_{vu} . $agg(\cdot)$ aggregates the messages $m_{vu}^{(k+1)}$ generated by $msg(\cdot)$ for each target node. $update(\cdot)$ updates the target node v to a new representation $h_v^{(k+1)}$ by combining the aggregated information $g_v^{(k+1)}$ with the previous embedding $h_v^{(k)}$. The embedding $h_v^{(k+1)}$ is used for prediction tasks or message passing in the next layer.

Since edges exist only between nodes from different sets (i.e., variable-constraint) in a MILP bipartite graph, obtaining a new representation for a decision variable requires two rounds of message passing. As shown in Figure 2(b), a new representation for the decision variables is obtained by performing one constraint-side convolution and one variable-side convolution after applying initial embeddings.



(a) Example of a bipartite graph representation for a MILP instance with three variables and two constraints.



(b) GCN for bipartite graph representation of MILP. V: Variable nodes, C: Constraint nodes, E: Edge features and adjacency matrix.

Figure 2: Bipartite graph for MILP and its GCN layers.

2.2.3. TRANSFORMER FOR GRAPHS

The Transformer (Vaswani, 2017), originally designed as a sequence-to-sequence model for machine translation, has achieved significant success in various domains such as NLP and computer vision. Recently, there have been numerous efforts to adapt Transformers for the graph domain (Lin et al., 2022; Min et al., 2022). The attention mechanism of Transformers enables each node to attend to every node, which allows the model to effectively learn relationships between distant nodes (Wu et al., 2021).

MPNN-based GNNs (MPNN, for short) receive messages from the neighbor node, which is suitable for learning local structural information. However, they struggle to capture relationships between distant nodes (Zhang et al., 2020; Wu et al., 2021). To propagate messages from nodes that are K hops away, a MPNN requires K layers. However, deeper layers can lead to oversmoothing, where nodes in a graph have similar and indistinguishable representations (Li et al., 2018; Wu et al., 2021; Min et al., 2022).

A MPNN for MILP may require deep layers to capture the relationships among variables that influence each other across multiple constraints. For instance, as illustrated in Figure 2(a), the variables x_2 and x_3 are 4 hops apart ($x_2 - \mathbf{a}_1 - x_1 - \mathbf{a}_2 - x_3$). Although x_2 and x_3 do not appear in the same constraint, they are connected via x_1 , which appears in both \mathbf{a}_1 and \mathbf{a}_2 . A change in the value of x_2 can affect x_1 , which may subsequently affect x_3 . Thus, capturing the relationship between these variables is essential. Propagating messages from x_2 to x_3 requires four GCN layers (see Figure 2). However, even a shallow MPNN with 2-4 layers can suffer from the oversmoothing (Wu et al., 2023). To address this, we utilize a Transformer-based GNN, which can effectively learn relationships among variables, regardless of their distance.

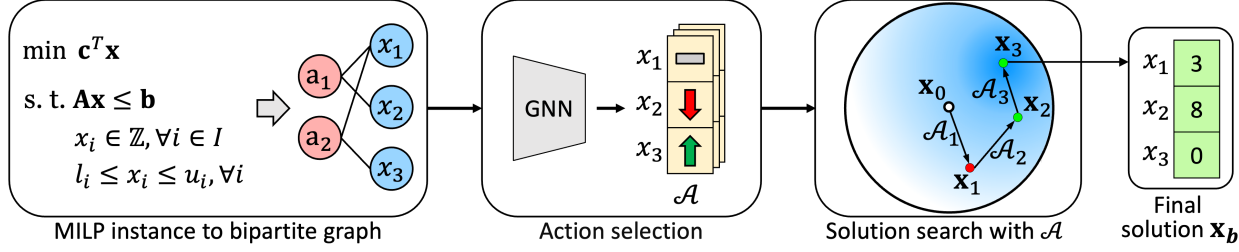


Figure 3: The overview of our approach. The symbols \uparrow , \downarrow , and $-$ denote an increase, a decrease, and no change in the values of decision variables, respectively. The white point (\mathbf{x}_0), red point (\mathbf{x}_1), and green points ($\mathbf{x}_2, \mathbf{x}_3$) denote the initial solution, an infeasible solution, and feasible solutions, respectively. The darker the area, the better the solutions.

3. Methodology

This section introduces the RL-MILP solver in detail. Figure 3 illustrates how our solver incrementally improves feasible solutions. The process begins with converting a given MILP instance into a bipartite graph. Next, the agent is trained on the graph to select high-reward actions. The selected actions derive a new solution \mathbf{x}_{t+1} . Finally, the current best solution \mathbf{x}_b is updated if \mathbf{x}_{t+1} is feasible and better than \mathbf{x}_b .

3.1. Reinforcement Learning for MILP

A RL system for MILP aims to train the agent to make decisions that maximize rewards while interacting with a given instance. Figure 4 depicts how the RL agent interacts with a MILP instance, where \mathcal{S}_t , \mathcal{A}_t , and $\mathcal{R}_{t,total}$ denote the observation, the set of selected actions, and the total reward at timestep t , respectively. The instance M acts as the environment for the agent. Using $\mathcal{A}_t = (a_{t,1}, \dots, a_{t,n})$, the agent updates the solution \mathbf{x}_{t+1} for n variables. This update affects the left-hand side of the constraints \mathbf{lhs}_{t+1} , the feasible state vector \mathbf{f}_{t+1} , and the objective value obj_{t+1} . At the next timestep, the agent faces a new observation \mathcal{S}_{t+1} changed by its previous actions and selects a new action set \mathcal{A}_{t+1} to maximize rewards. By comparing the actual reward $\mathcal{R}_{t+1,total}$ obtained from \mathcal{A}_{t+1} with the estimated reward, the agent refines its policy π .

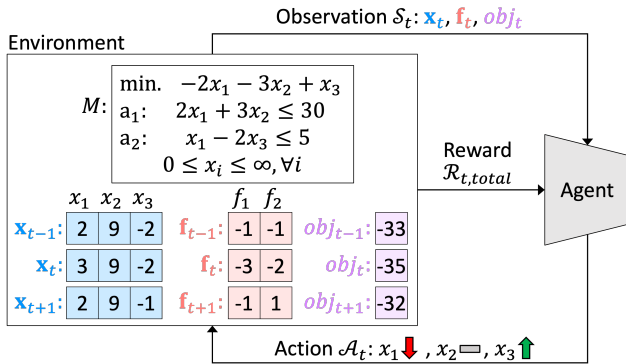


Figure 4: Diagram of reinforcement learning for MILP.

3.1.1. OBSERVATION

We define the observation $\mathcal{S}_t = (\mathbf{x}_t, \mathbf{f}_t, obj_t)$. The solution \mathbf{x}_t is derived by updating the values of variables based on the agent's actions \mathcal{A}_{t-1} . For example, assuming $\mathcal{A}_{t-1} = (a_{t-1,1}, a_{t-1,2}, a_{t-1,3}) = (+1, +0, +0)$, then \mathbf{x}_{t-1} in Figure 4 is updated to $\mathbf{x}_t = (x_{t,1}, x_{t,2}, x_{t,3}) = (3, 9, -2)$. With the updated \mathbf{x}_t , the new $\mathbf{lhs}_t = \mathbf{Ax}_t$ and $obj_t = \mathbf{c}^T \mathbf{x}_t$ are calculated.

Each elements of \mathbf{f}_t indicates whether \mathbf{x}_t satisfies the corresponding constraint, defined as $\mathbf{f}_t = \mathbf{b} - \mathbf{lhs}_t$. Non-negative elements in \mathbf{f}_t indicate satisfied constraints, while negative ones indicate violations. For example, in Figure 4, \mathbf{x}_{t+1} yields $\mathbf{lhs}_{t+1} = (31, 4)$ for constraints \mathbf{a}_1 and \mathbf{a}_2 . As $\mathbf{f}_{t+1} = \mathbf{b} - \mathbf{lhs}_{t+1} = (30, 5) - (31, 4) = (-1, 1)$, \mathbf{x}_{t+1} violates \mathbf{a}_1 but satisfies \mathbf{a}_2 .

3.1.2. ACTION

At timestep t , the agent selects a set of actions $\mathcal{A}_t = (a_{t,1}, \dots, a_{t,n})$ for n variables based on \mathcal{S}_t . For each variable, the agent can take one of three types of actions: increase, decrease, or no change, as shown in Figure 4.

3.1.3. REWARD

We design reward functions that enable the agent to select actions that maximize the total reward $\mathcal{R}_{t,total}$ in a given situation, as follows:

$$\mathcal{R}_{t,total} = \mathcal{R}_{t,opt} + \mathcal{R}_{t,explore} \quad (6)$$

Finding a feasible solution is a prerequisite for discovering the optimal solution. Therefore, the agent's primary objective is to find a feasible solution that satisfies all constraints. The feasibility reward $\mathcal{R}_{t,F}$ is calculated based on the constraint satisfaction and the upper/lower bound conditions of the decision variables, as follows:

$$\mathcal{R}_{t,F} = \frac{1}{\sqrt{mn}} \mathcal{R}_{t,const} + \frac{1}{\sqrt{n}} (\mathcal{R}_{t,ub} + \mathcal{R}_{t,lb}) \quad (7)$$

$$\mathcal{R}_{t,const} = \sum_{j=1}^m \min(f_{t+1,j}, 0) - \min(f_{t,j}, 0) \quad (8)$$

$$\mathcal{R}_{t,ub} = \sum_{i=1}^n \min(u_i - x_{t+1,i}, 0) - \min(u_i - x_{t,i}, 0) \quad (9)$$

$$\mathcal{R}_{t,lb} = \sum_{i=1}^n \min(x_{t+1,i} - l_i, 0) - \min(x_{t,i} - l_i, 0) \quad (10)$$

where $f_{t,j}$ is the element of \mathbf{f}_t for the j -th constraint, and $x_{t,i}$ of \mathbf{x}_t is the value of the i -th decision variable at timestep t . The constraint reward $\mathcal{R}_{t,const}$ is proportional to improvements (or deteriorations) for each infeasible constraint. For example, in Figure 4, $\mathcal{R}_{t,const}$ is $[\{-1 - (-3)\} + \{0 - (-2)\}] = 4$. The bound rewards $\mathcal{R}_{t,ub}$ and $\mathcal{R}_{t,lb}$ are proportional to changes for each variable that violates its bound conditions. As shown in Figure 4, $\mathcal{R}_{t,lb}$ is $[\{0 - 0\} + \{0 - 0\} + \{-1 - (-2)\}] = 1$ because the lower bound is 0, and $x_{t+1,3}$ improves by 1.

The reward system for our solver operates in two phases: *phase1* and *phase2*. *phase1* continues until the first feasible solution is found, while *phase2* begins thereafter. The optimization reward $\mathcal{R}_{t,opt}$ is calculated, as follows:

$$\mathcal{R}_{t,opt} = \begin{cases} \mathcal{R}_{t,p1}, & \text{if agent is in } phase1, \\ \mathcal{R}_{t,p2}, & \text{otherwise.} \end{cases} \quad (11)$$

$$\mathcal{R}_{t,p1} = \begin{cases} 1 - \delta_{t,r}, & \text{if } \mathbf{x}_{t+1} \in \mathcal{F}, \\ \mathcal{R}_{t,F}, & \text{otherwise.} \end{cases} \quad (12)$$

$$\mathcal{R}_{t,p2} = \begin{cases} (1 - \delta_{t,r}) \cdot \alpha, & \text{if } \mathbf{x}_{t+1} \in \mathcal{F} \wedge obj_{t+1} < obj_b, \\ 0, & \text{if } \mathbf{x}_{t+1} \in \mathcal{F} \wedge obj_{t+1} \geq obj_b, \\ \mathcal{R}_{t,F} \cdot \delta_{t,b} \cdot \beta, & \text{if } \mathbf{x}_{t+1} \notin \mathcal{F} \wedge obj_{t+1} < obj_b, \\ \mathcal{R}_{t,F} \cdot \delta_{t,b} & \text{otherwise.} \end{cases} \quad (13)$$

$$\delta_{t,r} = \frac{|obj_{t+1} - obj_r|}{|obj_r|}, \quad \delta_{t,b} = \frac{|obj_{t+1} - obj_b|}{|obj_r - obj_b|}. \quad (14)$$

where \mathcal{F} is the feasible region of a given MILP instance, $\alpha = 1/\beta$ and $\beta \in (0, 1]$ are toward-optimal bias parameters, and $\delta_{t,r}$ and $\delta_{t,b}$ are scaled gaps from obj_{t+1} to the lower bound obj_r and the current best objective value obj_b , respectively.

In *phase1*, the agent aims to find the first feasible solution. Achieving a better (i.e., lower) objective value in *phase1* sets the agent up for a better starting point in *phase2*. Thus, higher rewards are given as the solution nears obj_r (Eq. 12). If the agent finds an infeasible solution $\mathbf{x}_{t+1} \notin \mathcal{F}$, it is corrected by the feasibility reward $\mathcal{R}_{t,F}$. In *phase2*, the goal is to find feasible solutions better than the current best solution \mathbf{x}_b . If the agent finds better $\mathbf{x}_{t+1} \in \mathcal{F}$, it earns higher rewards as \mathbf{x}_{t+1} gets closer to obj_r (Case 1 in Eq. 13). For $\mathbf{x}_{t+1} \in \mathcal{F}$ worse than \mathbf{x}_b , the agent receives no reward due to no improvement and is also not penalized to avoid invalidating the learning from in *phase1* (Case 2 in Eq. 13). If $\mathbf{x}_{t+1} \notin \mathcal{F}$, the agent is encouraged to explore near \mathbf{x}_b

with smaller $\mathcal{R}_{t,F}$ as it gets closer to obj_b (Case 3, 4 in Eq. 13). According to Proposition 1, we regard $obj_{t+1} < obj_b$ as desirable; thus, the penalty is reduced by β (Case 3 in Eq. 13). Adjusting β further promote exploration toward obj_r .

To promote exploration, $\mathcal{R}_{t,explore}$ is calculated as follows:

$$\mathcal{R}_{t,explore} = \begin{cases} -10, & \text{if } \mathbf{x}_{t+1} = \mathbf{x}_t, \\ 0, & \text{otherwise.} \end{cases} \quad (15)$$

To prevent the agent from ceasing exploration, which is highly undesirable, the highest penalty of -10 is imposed.

3.1.4. LEARNING ALGORITHM

To train the RL agent, we adopt the Actor-Critic (AC) algorithm (Mnih et al., 2016), which has demonstrated effectiveness in solving CO problems (Bello et al., 2016; Hubbs et al., 2020). AC combines a policy-based actor and a value-based critic. The actor optimizes parameters θ to maximize the expected reward by learning a policy $\pi_\theta(\mathcal{A} | \mathcal{S})$ that maps the observation \mathcal{S} to a probability distribution over actions \mathcal{A} . The critic evaluates \mathcal{S} by learning a value function $V_\theta(\mathcal{S})$, which estimates expected return for a given \mathcal{S} .

At each timestep t , the agent observes \mathcal{S}_t and selects actions \mathcal{A}_t using the policy π . Upon executing \mathcal{A}_t , the environment reacts by providing a observed reward $\mathcal{R}_{t,total}$ and \mathcal{S}_{t+1} . The actor is trained to encourage actions with higher $\mathcal{R}_{t,total}$ than the estimated value $V_\theta(\mathcal{S}_t)$ and suppress those with lower $\mathcal{R}_{t,total}$. The critic is trained to minimize the gap between \mathcal{R}_t and $V_\theta(\mathcal{S}_t)$ to provide accurate feedback to the actor.

To train the RL agent across diverse environments, we expose it to randomly generated MILP instances. To ensure sufficient training in *phase1*, we enforce the agent stays in *phase1* for the predefined number of steps, even after finding the first feasible solution. Training proceeds until the agent reaches the total step limit, finds the optimal solution, or fails to improve solutions in *phase2* within the grace period. Once any condition is met, the agent switches to a new instance. Appendix C presents the pseudo-code.

3.2. GNN Architecture of RL Agent

We adopt a hybrid approach combining a MPNN with a Transformer encoder (Rong et al., 2020; Wu et al., 2021) for the RL agent, as shown in Figure 5. The MPNN captures local information for each decision variable. Local information can include whether the constraints involving a variable are satisfied. To learn local information, we use the following features: \mathbf{x}_t for variable nodes, \mathbf{b} for constraint nodes, and \mathbf{A} for edges. To ensure stable training, we scale \mathbf{A} to $[-1, 1]$ using equilibration scaling (Tomlin, 1975), which normalizes each constraint by its largest absolute coefficient. This scaling relies on the principle that multiplying each constraint by a positive scalar produces an

equivalent LP problem to the original. For \mathbf{x}_t and \mathbf{b} , which may have unbounded values, we use a Periodic Embedding (PE) (Gorishniy et al., 2022) module to embed scalars into vectors. PE has demonstrated effectiveness in deep learning models for processing numerical features, including tasks such as house price and income prediction (Pace & Barry, 1997; Kohavi et al., 1996). PE is formulated as follows:

$$\text{PE}(z) = \oplus(\sin(\tilde{z}), \cos(\tilde{z})), \quad \tilde{z} = [2\pi w_1 z, \dots, 2\pi w_k z].$$

where $\oplus(\cdot)$ is concatenation, with scalar z and trainable w_i .

We utilize the Transformer encoder to enable the agent to capture global information of MILP. Global information may include relationships among variables connected via multiple constraints, and feasibility. As shown in Figure 5, the encoder takes the following vectors as input: a phase token [PHA], PE-encoded obj_r and obj_b , scaled \mathbf{f}_t , and $\tilde{\mathbf{h}}_{v,t}^{(L)}$. \mathbf{f}_t is scaled by $\sqrt{|\mathbf{b}| + |\mathbf{b} - \mathbf{l}\mathbf{h}\mathbf{s}_t|}$. The vector $\tilde{\mathbf{h}}_{v,t}^{(L)} = \oplus(h_{v,t}^{(L)}, h_{v,t}^{(0)}, \text{bnd_lim}, (\mathbf{c}|\mathbf{A}^T))$ represents decision variable embeddings, where $(\mathbf{c}|\mathbf{A}^T)$ contains structural information of the graph, and bnd_lim is a binary feature. bnd_lim is set to 1 if a variable’s value of \mathbf{x}_t reaches or exceeds its bound, otherwise 0. For example, if $x_j = 0$ and $x_k = 5$ with a lower bound of 0, the bnd_lim for x_j and x_k would be 1 and 0, respectively. [PHA] informs the agent of its current phase. As explained in Section 3.1.3, since the two phases have distinct goals, the same actions can yield different rewards depending on the phase. Without phase awareness, the agent may take unsuitable actions. For example, instead of exploring better feasible solutions within the interval (i.e., $obj_{t+1} \in [obj_r, obj_b]$) in *phase2*, the agent might stay outside the interval. [PHA] can prevent such behavior by guiding the agent based on the current phase.

The Actor layer generates \mathcal{A}_t using the final embeddings for decision variables. The Critic layer approximates the expected return function using the embeddings for [PHA], obj_r , obj_b , and \mathbf{f}_t . These embeddings are used because the total reward depends on the solution quality and feasibility improvements or deteriorations (see Eq. 6). Since the reward system differs between *phase1* and *phase2*, the Actor and Critic layers are separated by phase, while all other layers share parameters across the two phases.

3.3. Solution Search Strategy

Our search strategy is inspired by local search (LS), a widely used heuristic that explores the neighbors of the current solution for CO problems (Bertsimas & Tsitsiklis, 1997; Hillier & Lieberman, 2015). While LS may encounter local optima, empirical evidence suggests that it is effective at quickly finding quality solutions (Bertsimas & Tsitsiklis, 1997). Classic LS randomly tweaks one variable at a time, but moving farther in each step can be more effective (Shaw, 1998). In contrast to the classic LS, our search strat-

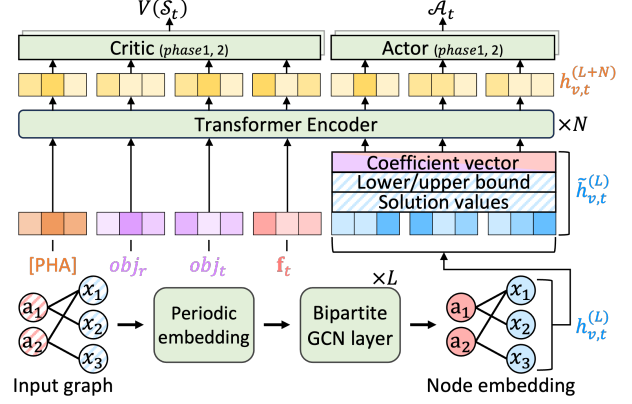


Figure 5: The GNN architecture for solving MILP.

egy imposes no restrictions on the number of variables that can change per step. Thus, the RL-MILP solver explores a larger neighborhood than LS conceptually. Moreover, the magnitude of the changes can be adjusted by expanding the number of the agent’s possible actions. For instance, each variable can have three possible actions (+1, 0, -1) or five (+2, +1, 0, -1, -2). Our approach employs a trained RL agent to navigate the solution space toward the optimal solution. The agent selects actions expected to yield higher rewards based on new observations. During *phase1*, the agent searches within a local region, whereas in *phase2*, it moves only to feasible solutions with better or equal objective values. Appendix D provides the pseudo-code.

4. Experiments

We conduct experiments to answer these research questions:

- RQ1: How accurately does RL-MILP solver approximate solutions in terms of solution quality?
- RQ2: How does the toward-optimal bias parameter β influence the solution quality?
- RQ3: How effective is the proposed GNN architecture compared to alternative architectures in solving MILP?

4.1. Experimental Setup

4.1.1. DATASET COLLECTION

We generated MILP instances based on the description in (Qi et al., 2021). Our study focuses on a special case of MILP where all variables are integers to emphasize handling integer variables. Datasets are named $D_{n \times m}$, where n and m are the numbers of variables and constraints, respectively. We use $D_{9 \times 18}$, $D_{50 \times 20}$, $D_{100 \times 50}$, and $D_{300 \times 100}$, where $D_{300 \times 100}$ is approximately 185 times larger than $D_{9 \times 18}$ that matches the largest dataset from (Qi et al., 2021). We generated 100 instances for each dataset for the test phase. Appendix E.1 details the data generation process.

Table 1: Evaluation results for combination of $D_{n \times m}$ and β with three possible actions (+1, 0, -1). Bold text indicates the best Gap with 100% FR for each combination, while * marks the dataset-wise best among them. “N/A” denotes that calculation is not applicable. FFST for Gurobi is represented as “< t ” because sub-second timing was unavailable in logs.

Method		$D_{9 \times 18}$			$D_{50 \times 20}$			$D_{100 \times 50}$			$D_{300 \times 100}$		
		FR \uparrow	FFST \downarrow	Gap \downarrow	FR \uparrow	FFST \downarrow	Gap \downarrow	FR \uparrow	FFST \downarrow	Gap \downarrow	FR \uparrow	FFST \downarrow	Gap \downarrow
Gurobi		100%	< 1s	0.00%	100%	< 1s	0.00%	100%	< 1s	0.01%	100%	< 1s	0.03%
$\beta = 1$	LS	-	-	0.07%	-	-	0.09%	-	-	0.57%	-	-	0.78%
	M_MLP	100%	0.05s	0.01%	87%	0.06s	0.12%	99%	0.06s	0.52%	97%	0.10s	0.64%
	M_CNN	100%	0.06s	0.01%	1%	0.06s	0.05%	0%	N/A	N/A	0%	N/A	N/A
	Ours	100%	0.05s	0.15%	100%	0.05s	0.09%	100%	0.07s	0.55%	100%	0.13s	0.45%
$\beta = 0.6$	LS	-	-	0.07%	-	-	0.08%	-	-	0.58%	-	-	0.69%
	M_MLP	100%	0.05s	0.02%	100%	0.05s	0.12%	99%	0.06s	0.51%	97%	0.10s	0.65%
	M_CNN	100%	0.06s	0.00%*	3%	0.04s	0.01%	0%	N/A	N/A	0%	N/A	N/A
	Ours	100%	0.05s	0.00%*	100%	0.05s	0.08%	100%	0.09s	0.38%	100%	0.11s	0.41%*
$\beta = 0.3$	LS	-	-	0.07%	-	-	0.08%	-	-	0.57%	-	-	0.72%
	M_MLP	100%	0.05s	0.00%*	100%	0.05s	0.11%	100%	0.06s	0.40%	99%	0.11s	0.65%
	M_CNN	100%	0.06s	0.01%	4%	0.04s	0.03%	0%	N/A	N/A	0%	N/A	N/A
	Ours	100%	0.05s	0.00%*	100%	0.05s	0.07%*	100%	0.06s	0.34%*	100%	0.11s	0.47%

4.1.2. COMPARED METHODS

For RQ1, we evaluated the RL-MILP solver against the SOTA commercial optimizer, Gurobi, and the classic local search (LS). LS starts in *phase2* from a feasible solution provided by the trained RL agent in *phase1*, as it requires a feasible starting point (Bertsimas & Tsitsiklis, 1997). For RQ3, we evaluated our method against two baselines: M_MLP and M_CNN. These baselines adopt Multi-layer perceptron (MLP) and Convolutional neural network (CNN), as shown effective in finding a feasible solution (Qi et al., 2021). The MLP and CNN substitute for the Transformer encoder in Figure 5, and they are referred to as M_MLP and M_CNN, respectively. For RQ2, the compared methods were trained with different β settings. Existing partial end-to-end learning methods lack support for integer variables and are not standalone solvers; hence, they were excluded. Each method solves a given MILP instance within 100 seconds.

4.1.3. METRICS

For feasibility evaluation, we introduce *Feasible rate* (FR) and *First feasible solution time* (FFST). FR measures the ratio of instances where a feasible solution is found. FFST records the time taken to obtain the first feasible solution. For solution quality, we use *Relative primal gap* (Gap) (Gasse et al., 2022) and #win. Gap quantifies how close a method’s best objective value obj_b is to the best-known value. Gap is calculated as $\text{Gap} = \frac{|obj_b - BKS|}{|BKS|} * 100$, where BKS is the best value obtained among all compared methods, including Gurobi with a 600-second time limit. #win measures the number of test instances where a method reaches the best value obtained among all compared methods. In case of a tie, each method receives a count for #win.

4.2. Main Results

The results in Table 1 show that the RL-MILP solver accurately finds feasible solutions and achieves (near-)optimal solutions. It consistently finds the first feasible solutions within 1 second across all instances and combinations of $D_{n \times m}$ and β . Additionally, it reaches optimal objective values on $D_{9 \times 18}$ and near-optimal values on larger datasets, maintaining a Gap below 1%.

With a toward-optimal bias (i.e., $\beta = \{0.3, 0.6\}$), the compared methods tend to find better solutions. The agent chooses the lesser of two evils, as the potential penalty for solutions with $obj_{t+1} < obj_b$ is lower than for those with $obj_{t+1} \geq obj_b$ (see Figure 7 in Appendix B). Interestingly, the RL-MILP solver with $\beta = 1$ on $D_{9 \times 18}$ exhibits the worst Gap among the compared methods, as $\beta = 1$ implies no toward-optimal bias. Thus, a suitable toward-optimal bias promotes exploration toward obj_r , enhancing solution quality. This empirical evidence highlights the importance of guiding the agent’s search, supporting Proposition 1.

Comparing the RL-MILP solver with LS directly highlights search performances in *phase2*. Since LS begins *phase2* from a feasible solution provided by the RL-MILP solver, feasibility evaluation for LS is omitted. Even on the smallest dataset $D_{9 \times 18}$, LS fails to reach the optimal solution, unlike the RL-MILP solver whose neighborhood set is larger.

The RL-MILP solver achieves the lowest Gap with a 100% FR across all datasets, outperforming the baselines, while M_MLP and M_CNN struggle as dataset size increases. These results suggest that the attention mechanism effectively captures variable-constraint interactions and relationships between distant nodes even in larger datasets.

Table 2: Performance by neighborhood sizes on $D_{100 \times 50}$. All methods achieves FFST under 1 second.

Method	Δ_x	$\beta = 0.5$			$\beta = 0.8$		
		FR \uparrow	Gap \downarrow	#win \uparrow	FR \uparrow	Gap \downarrow	#win \uparrow
LS	1	100%	0.58%	2	100%	0.58%	0
Ours	1	100%	0.36%	21	100%	0.36%	14
	3	100%	0.31%	40	99%	0.32%	37
	5	100%	0.31%	50	100%	0.30%	55

4.3. Impact of Varying Neighborhood Sizes

Inspired by the insight that moving farther can overcome barriers created by numerous constraints in the search space (Shaw, 1998), we examine the effect of the agent’s movement magnitude per step on the performance. In this experiment, we extend the solving time to 300 seconds, providing sufficient time for the agent to escape local optima. The neighborhood size grows as the number of changeable variables n_x per step and the maximum magnitude of change for variables Δ_x increase. Table 2 shows the impact of varying the neighborhood size. The RL-MILP solver with $\Delta_x = 1$ achieves a lower Gap than LS with its larger $n_x = n$ than LS’s $n_x = 1$. Furthermore, the highest #win is obtained with $\Delta_x = 5$, which is the largest action set (+5, +4, +3, +2, +1, 0, -1, -2, -3, -4, -5) in this experiment. This suggests that expanding the neighborhood size enhances the RL-MILP solver’s ability to overcome local optima. As noted in previous research (Son et al., 2023), ensuring the optimality of neural networks for CO problems remains an open challenge due to the lack of theoretical guarantees. This result suggests a promising direction for exploring the optimality of RL-based solvers for MILP problems.

4.4. Ablation Studies

We conducted an ablation study to evaluate the effectiveness of the following components: Transformer encoder (TE),

 Table 3: Ablation study of the proposed GNN architecture on $D_{100 \times 50}$ with $\beta = 0.6$ and three possible actions.

Ablation Settings					Metric	
TE	MP	PE	SL	PT	FR \uparrow	Gap \downarrow
	✓	✓	✓	✓	100%	0.59%
✓		✓	✓	✓	99%	0.49%
✓	✓				98%	2.82%
✓	✓	✓			99%	2.69%
✓	✓	✓	✓		100%	0.42%
✓	✓	✓	✓	✓	100%	0.38%

MPNN (MP), Periodic embedding (PE), Separated layers (SL), and [PHA] token (PT), illustrated in Figure 5. As shown in Table 3, comparing the removal of TE with the removal of MP, the latter leads improvement in Gap but a loss in FR. Although TE improves Gap, this result emphasizes the importance of MP in capturing local information such as feasibility. Combining all components achieves the best performance in terms of Gap and FR, with SL contributing substantial improvement.

5. Related Work

Bengio et al. (2021) have categorized ML techniques for solving CO into three groups. The first group, *Learning to Configure Algorithms*, leverages ML to optimize the configuration of specific techniques in traditional solvers. For instance, ML improves solving speed by deciding whether to execute specific operations, such as decomposition (Kruber et al., 2017). The second group, *Machine Learning Alongside Optimization Algorithms*, integrates ML into traditional solvers to aid key decisions during the optimization process (e.g., selecting the next search region (Lodi & Zarpellon, 2017)). The third group, *End-to-End Learning*, uses ML to directly learn and predict solutions. This group includes ML-based primal heuristics (Gasse et al., 2019; Nair et al., 2020; Yoon, 2022; Han et al., 2023; Cantürk et al., 2024), as well as our method. Existing ML-based primal heuristics output only partial solutions and face challenges in handling non-binary integer variables. They also rely on costly supervised learning for labeled data. A previous RL-based study on MILP focuses solely on finding the first feasible solution (Qi et al., 2021) without optimizing further. To our knowledge, this study is the first full end-to-end RL-based solver that improves solution quality for MILP involving integer variables without relying on traditional solvers.

6. Conclusion

In this study, we introduced a novel RL-MILP solver that generates complete feasible solutions without delegating sub-problems to traditional solvers. We designed an RL system that enables the agent to learn MILP problem-solving by capturing variable-constraint relationships. Building on theoretical insights, we guide the RL agent’s solution search by designing a structured reward mechanism and a search strategy. To enhance problem-solving capabilities, we proposed a Transformer-based GNN architecture for the RL-MILP solver. Experimental results show that the RL-MILP solver quickly finds the first feasible solution and improves solution quality toward optimality. The RL-MILP solver achieves optimal solutions for a small dataset and near-optimal solutions with a Gap of less than 1% for larger datasets. This study lays the groundwork for full end-to-end RL-driven approaches to MILP problem-solving.

Acknowledgements

This work was supported by the Institute of Information & communications Technology Planning & Evaluation (IITP) grant funded by the Korea government(MSIT) (No. 2019-0-01267, GPU-based Ultrafast Multi-type Graph Database Engine SW).

References

- Achterberg, T., Berthold, T., and Hendel, G. Rounding and propagation heuristics for mixed integer programming. In *Operations Research Proceedings 2011: Selected Papers of the International Conference on Operations Research (OR 2011), August 30-September 2, 2011, Zurich, Switzerland*, pp. 71–76. Springer, 2012.
- Bello, I., Pham, H., Le, Q. V., Norouzi, M., and Bengio, S. Neural combinatorial optimization with reinforcement learning. *arXiv preprint arXiv:1611.09940*, 2016.
- Bengio, Y., Lodi, A., and Prouvost, A. Machine learning for combinatorial optimization: a methodological tour d’horizon. *European Journal of Operational Research*, 290(2):405–421, 2021.
- Bertsimas, D. and Tsitsiklis, J. N. *Introduction to linear optimization*, volume 6. Athena Scientific Belmont, MA, 1997.
- Cantürk, F., Varol, T., Aydoğan, R., and Özener, O. Ö. Scalable primal heuristics using graph neural networks for combinatorial optimization. *Journal of Artificial Intelligence Research*, 80:327–376, 2024.
- Cont, R. and Heidari, M. Optimal rounding under integer constraints. *arXiv preprint arXiv:1501.00014*, 2014.
- Fischetti, M., Glover, F., and Lodi, A. The feasibility pump. *Mathematical Programming*, 104:91–104, 2005.
- Floudas, C. A. *Nonlinear and mixed-integer optimization: fundamentals and applications*. Oxford University Press, 1995.
- Gasse, M., Chételat, D., Ferroni, N., Charlin, L., and Lodi, A. Exact combinatorial optimization with graph convolutional neural networks. *Advances in neural information processing systems*, 32, 2019.
- Gasse, M., Bowly, S., Cappart, Q., Charfreitag, J., Charlin, L., Chételat, D., Chmiela, A., Dumouchelle, J., Gleixner, A., Kazachkov, A. M., et al. The machine learning for combinatorial optimization competition (ml4co): Results and insights. In *NeurIPS 2021 competitions and demonstrations track*, pp. 220–231. PMLR, 2022.
- Gilmer, J., Schoenholz, S. S., Riley, P. F., Vinyals, O., and Dahl, G. E. Neural message passing for quantum chemistry. In *Proceedings of the 34th International Conference on Machine Learning - Volume 70, ICML’17*, pp. 1263–1272. JMLR.org, 2017.
- Gorishniy, Y., Rubachev, I., and Babenko, A. On embeddings for numerical features in tabular deep learning. *Advances in Neural Information Processing Systems*, 35: 24991–25004, 2022.
- Guieu, O. and Chinneck, J. W. Analyzing infeasible mixed-integer and integer linear programs. *INFORMS Journal on Computing*, 11(1):63–77, 1999.
- Gurobi Optimization, L. Gurobi optimizer reference manual. <https://docs.gurobi.com/projects/optimizer>, 2025.
- Han, Q., Yang, L., Chen, Q., Zhou, X., Zhang, D., Wang, A., Sun, R., and Luo, X. A gnn-guided predict-and-search framework for mixed-integer linear programming. In *The Eleventh International Conference on Learning Representations*, 2023.
- Hillier, F. S. and Lieberman, G. J. *Introduction to operations research*. McGraw-Hill, 2015.
- Hubbs, C. D., Li, C., Sahinidis, N. V., Grossmann, I. E., and Wassick, J. M. A deep reinforcement learning approach for chemical production scheduling. *Computers & Chemical Engineering*, 141:106982, 2020.
- Kipf, T. N. and Welling, M. Semi-supervised classification with graph convolutional networks. In *International Conference on Learning Representations*, 2017. URL <https://openreview.net/forum?id=SJU4ayYgl>.
- Kohavi, R. et al. Scaling up the accuracy of naive-bayes classifiers: A decision-tree hybrid. In *Kdd*, volume 96, pp. 202–207, 1996.
- Kostrikov, I. Pytorch implementations of reinforcement learning algorithms. <https://github.com/ikostrikov/pytorch-a2c-ppo-acktr-gail>, 2018.
- Kruber, M., Lübbecke, M. E., and Parmentier, A. Learning when to use a decomposition. In *International conference on AI and OR techniques in constraint programming for combinatorial optimization problems*, pp. 202–210. Springer, 2017.
- Kweon, O., Kim, B.-I., Lee, G., Im, H., Chung, C. Y., and Lim, O. K. Parcel delivery network optimization problem considering multiple hubs and consolidation of small-sized parcels. *Computers & Industrial Engineering*, 191: 110113, 2024.

- Land, A. H. and Doig, A. G. *An automatic method for solving discrete programming problems*. Springer, 2010.
- Li, Q., Han, Z., and Wu, X.-M. Deeper insights into graph convolutional networks for semi-supervised learning. In *Proceedings of the AAAI conference on artificial intelligence*, volume 32(1), 2018.
- Lin, T., Wang, Y., Liu, X., and Qiu, X. A survey of transformers. *AI open*, 3:111–132, 2022.
- Liu, F., Lin, X., Wang, Z., Zhang, Q., Xialiang, T., and Yuan, M. Multi-task learning for routing problem with cross-problem zero-shot generalization. In *Proceedings of the 30th ACM SIGKDD Conference on Knowledge Discovery and Data Mining*, pp. 1898–1908, 2024.
- Lodi, A. and Zarpellon, G. On learning and branching: a survey. *Top*, 25:207–236, 2017.
- Martin, R. K. *Large scale linear and integer optimization: a unified approach*. Springer Science & Business Media, 2012.
- Mazyavkina, N., Sviridov, S., Ivanov, S., and Burnaev, E. Reinforcement learning for combinatorial optimization: A survey. *Computers & Operations Research*, 134: 105400, 2021.
- Min, E., Chen, R., Bian, Y., Xu, T., Zhao, K., Huang, W., Zhao, P., Huang, J., Ananiadou, S., and Rong, Y. Transformer for graphs: An overview from architecture perspective. *arXiv preprint arXiv:2202.08455*, 2022.
- Mnih, V., Badia, A. P., Mirza, M., Graves, A., Lillicrap, T., Harley, T., Silver, D., and Kavukcuoglu, K. Asynchronous methods for deep reinforcement learning. In Balcan, M. F. and Weinberger, K. Q. (eds.), *Proceedings of The 33rd International Conference on Machine Learning*, volume 48 of *Proceedings of Machine Learning Research*, pp. 1928–1937, New York, New York, USA, 20–22 Jun 2016. PMLR.
- Nair, V., Bartunov, S., Gimeno, F., Von Glehn, I., Lichocki, P., Lobov, I., O’Donoghue, B., Sonnerat, N., Tjandraatmadja, C., Wang, P., et al. Solving mixed integer programs using neural networks. *arXiv preprint arXiv:2012.13349*, 2020.
- Pace, R. K. and Barry, R. Sparse spatial autoregressions. *Statistics & Probability Letters*, 33(3):291–297, 1997.
- Papageorgiou, D. J., Nemhauser, G. L., Sokol, J., Cheon, M.-S., and Keha, A. B. Mirplib—a library of maritime inventory routing problem instances: Survey, core model, and benchmark results. *European Journal of Operational Research*, 235(2):350–366, 2014.
- Qi, M., Wang, M., and Shen, Z.-J. Smart feasibility pump: Reinforcement learning for (mixed) integer programming. *arXiv preprint arXiv:2102.09663*, 2021.
- Ren, H. and Gao, W. A milp model for integrated plan and evaluation of distributed energy systems. *Applied energy*, 87(3):1001–1014, 2010.
- Rong, Y., Bian, Y., Xu, T., Xie, W., Wei, Y., Huang, W., and Huang, J. Self-supervised graph transformer on large-scale molecular data. *Advances in neural information processing systems*, 33:12559–12571, 2020.
- Shaw, P. Using constraint programming and local search methods to solve vehicle routing problems. In *International conference on principles and practice of constraint programming*, pp. 417–431. Springer, 1998.
- Son, J., Kim, M., Kim, H., and Park, J. Meta-sage: Scale meta-learning scheduled adaptation with guided exploration for mitigating scale shift on combinatorial optimization. In *International Conference on Machine Learning*, pp. 32194–32210. PMLR, 2023.
- Tomlin, J. A. *On scaling linear programming problems*. Springer, 1975.
- Vaswani, A. Attention is all you need. *Advances in Neural Information Processing Systems*, 2017.
- Veličković, P., Cucurull, G., Casanova, A., Romero, A., Liò, P., and Bengio, Y. Graph attention networks. In *International Conference on Learning Representations*, 2018. URL <https://openreview.net/forum?id=rJXMpikCZ>.
- Witzig, J., Berthold, T., and Heinz, S. Computational aspects of infeasibility analysis in mixed integer programming. *Mathematical Programming Computation*, 13(4): 753–785, 2021.
- Wu, X., Chen, Z., Wang, W. W., and Jadbabaie, A. A non-asymptotic analysis of oversmoothing in graph neural networks. In *The Eleventh International Conference on Learning Representations*, 2023.
- Wu, Z., Jain, P., Wright, M., Mirhoseini, A., Gonzalez, J. E., and Stoica, I. Representing long-range context for graph neural networks with global attention. *Advances in Neural Information Processing Systems*, 34:13266–13279, 2021.
- Xu, K., Hu, W., Leskovec, J., and Jegelka, S. How powerful are graph neural networks? In *International Conference on Learning Representations*, 2019. URL <https://openreview.net/forum?id=ryGs6iA5Km>.
- Yoon, T. Confidence threshold neural diving. *arXiv preprint arXiv:2202.07506*, 2022.

Zhang, J., Zhang, H., Xia, C., and Sun, L. Graph-bert: Only attention is needed for learning graph representations. *arXiv preprint arXiv:2001.05140*, 2020.

Zuo, Y., Tharmarasa, R., Jassemi-Zargani, R., Kashyap, N., Thiyaalingam, J., and Kirubarajan, T. T. Milp formulation for aircraft path planning in persistent surveillance. *IEEE Transactions on Aerospace and Electronic Systems*, 56(5):3796–3811, 2020.

A. Proof of Proposition 1

In this section, we prove Proposition 1: *If a better feasible solution \mathbf{x}' exists for a given MILP problem, \mathbf{x}' must yield obj' that lies between obj_r and obj_b .*

A.1. Term Definitions

- \mathcal{F}_{MILP} : The set of feasible solutions (feasible region) for the given original MILP problem.
- \mathcal{F}_{LP} : The set of feasible solutions (feasible region) for the LP-relaxed problem of the original MILP problem.
- \mathbf{x}_r : The optimal solution of the LP-relaxed problem.
- \mathbf{x}_{opt} : The optimal solution of the original MILP problem.
- \mathbf{x}_b : The current best feasible solution of the original MILP problem.
- \mathbf{x}' : A better feasible solution than \mathbf{x}_b .
- obj_r : The optimal value obtained by \mathbf{x}_r .
- obj_{opt} : The optimal value obtained by \mathbf{x}_{opt} .
- obj_b : The objective value obtained by \mathbf{x}_b .
- obj' : The objective value obtained by \mathbf{x}' .

A.2. Background

Adding a constraint to a LP problem introduces a new boundary to the feasible region. The new boundary either reduces the size of the feasible region or leaves it unchanged. As previously mentioned in Section 1, A LP problem becomes a MILP problem if integrality requirements are added. Consequently, a MILP problem has more constraints than its LP-relaxed problem, establishing the relationship $\mathcal{F}_{MILP} \subseteq \mathcal{F}_{LP}$ (Guieu & Chinneck, 1999). Due to this relationship, feasible solutions to the original MILP problem are also feasible for its LP-relaxed problem. Hence, the optimal solution \mathbf{x}_{opt} for the original MILP problem lies within the feasible region of the LP-relaxed problem (i.e., $\mathbf{x}_{opt} \in \mathcal{F}_{LP}$). In the feasible region of the LP-relaxed problem excluding \mathcal{F}_{MILP} (i.e., $\mathcal{F}_{LP} - \mathcal{F}_{MILP}$), there may exist solutions that yield better (i.e., smaller for minimization problems) objective values than \mathbf{x}_{opt} . Therefore, in minimization problems, the inequality $obj_r \leq obj_{opt}$ holds (Martin, 2012).

A.3. Proof

Assumption 1. $\mathbf{x}_b \neq \mathbf{x}_{opt}$

Under Assumption 1, at least one better feasible solution \mathbf{x}' exists. According to the definitions provided in Section A.1, \mathbf{x}' represents a better solution than \mathbf{x}_b . Since we are dealing with a minimization problem, it follows that $obj' < obj_b$. Additionally, by the definitions in Section A.1, \mathbf{x}_{opt} is the optimal solution for the original MILP problem, which implies $obj_{opt} \leq obj' < obj_b$. As explained in Section A.2, $obj_r \leq obj_{opt}$ holds, establishing that obj_r serves as the lower bound for the original MILP problem in a minimization context. Consequently, the relationship $obj_r \leq obj_{opt} \leq obj' < obj_b$ is valid. Hence, since obj' derived from \mathbf{x}' always falls within the range of obj_r and obj_b , Proposition 1 holds true.

B. Visual Explanation of Reward Function in *phase2*

This section provides a detailed explanation of the reward function in *phase2* (Eq. 13) with visual aids. If a better objective value than obj_b exists, it must lie between the lower bound obj_r and obj_b (see Appendix A). Thus, the agent should explore solutions within this interval (i.e., $obj_{t+1} \in [obj_r, obj_b]$) to obtain a better solution. As obj_{t+1} approaches obj_r , the objective value improves; however, the feasibility becomes more challenging due to tighter constraints. Therefore, we encourage the agent to explore solutions near the current best feasible solution obj_b .

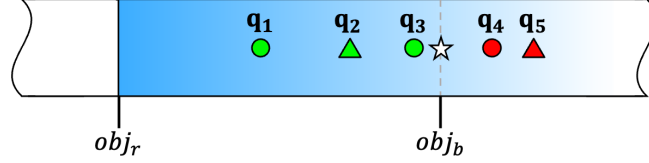


Figure 6: Illustration of reward function in *phase2*. \circ : feasible, \triangle : infeasible, green: inside, red: outside, \star : obj_b .

The green circles in Figure 6 correspond to better feasible solutions whose objective values is $obj_{t+1} < obj_b$ (Case 1 in Eq. 13). We regard the agent's actions that fail to find better feasible solutions than \mathbf{x}_b as incorrect actions. However, feasible solutions outside the interval are neither rewarded nor penalized (Case 2). The reason is not only that such solutions fail to improve solution quality but also that applying penalties could undermine the learning achieved in *phase1*. To maintain consistency with the learning from *phase1*, at least no penalties are imposed on feasible solutions outside the interval. For infeasible solutions, the agent is penalized in proportion to the gap between obj_{t+1} and obj_b (Case 3, 4), which corresponds to all triangles. To guide the agent toward the optimal objective value, infeasible solutions with $obj_{t+1} < obj_b$ (green triangle) are penalized less than the ones with $obj_{t+1} \geq obj_b$ (red triangle) by applying $\beta \in (0, 1]$ (Case 3).

Let the objective values be $obj_r = -20$, $obj_b = -10$, $q_1 = -16$, $q_2 = -13$, $q_3 = -11$, $q_4 = -8$, $q_5 = -7$, $\alpha = 2$, and $\beta = 0.5$. For the green circles, rewards in *phase2* are calculated by the first case in Eq. 13. The reward for q_1 is $(1 - \frac{|-16 - (-20)|}{|-20|}) \cdot \alpha = 0.8 \cdot 2 = 1.6$. The reward for q_3 is $(1 - \frac{|-11 - (-20)|}{|-20|}) \cdot \alpha = 0.55 \cdot 2 = 1.1$. Since q_1 is closer to the lower bound compared to q_3 , it receives a higher reward. For the red circle, the reward is 0 by the second case. For the green triangle, the penalty is calculated using the third case. The penalty for q_2 is $\mathcal{R}_{t,F} \cdot \frac{|-13 - (-10)|}{|-20 - (-10)|} \cdot \beta = \mathcal{R}_{t,F} \cdot 0.15$. For the red triangle, the penalty is calculated using the fourth case. The penalty for q_5 is $\mathcal{R}_{t,F} \cdot \frac{|-7 - (-10)|}{|-20 - (-10)|} = \mathcal{R}_{t,F} \cdot 0.3$. The distances from obj_b to q_2 and q_5 are the same (i.e., $|-13 - (-10)| = |-7 - (-10)| = 3$), but the penalty for q_2 is smaller than that for q_5 due to scaling by β .

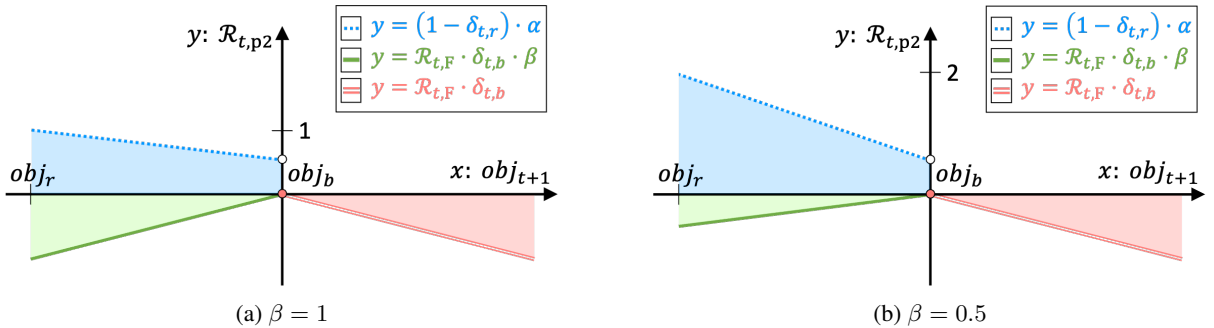


Figure 7: Illustration of the potential rewards of $\mathcal{R}_{t,p2}$ as a function of the objective value obj_{t+1} in *phase2*. The x -axis represents obj_{t+1} , and the y -axis represents $\mathcal{R}_{t,p2}$, with the origin set at obj_b . Assume that $\mathcal{R}_{t,F}$ remains constant.

Figure 7 visualizes the agent's potential rewards in *phase2*. The second quadrant represents rewards for solutions with $obj_{t+1} < obj_b$, which increase as they approach the lower bound obj_r . The third and fourth quadrants illustrate penalties that increase with the distance of infeasible solutions from the current best objective value obj_b , assuming $\mathcal{R}_{t,F}$ as a constant for simplicity. When obj_{t+1} is the same as obj_b , the penalty becomes zero, but the agent incurs a penalty of -10 only if the agent takes no action (i.e., $\mathbf{x}_t = \mathbf{x}_{t+1}$ in Eq. 15). As illustrated in Figures 7(a) and 7(b), a lower β (higher α) results in higher potential rewards and reduced penalties for solutions with $obj_{t+1} < obj_b$. We can promote the agent to take actions that lead to solutions with $obj_{t+1} < obj_b$ by controlling the toward-optimal bias parameters α and β .

C. Pseudo-Code for Learning Algorithm

Algorithm 1 Learning a Policy for RL-MILP Solver using Actor-Critic Algorithm

Input: Agent parameters θ

Parameter: Update limit N , Total step limit T_{max} , Warm-up step limit T_{warm} , Grace period T_{grace} , Data parameters \mathcal{P}

Output: Updated parameters θ

```

1: for  $N$  updates do
2:    $M \leftarrow \text{GetNewInstance}(\mathcal{P})$  {See Appendix E.1}
3:    $\mathbf{x}_0, obj_r \leftarrow \text{Relaxation}(M)$ 
4:    $\mathcal{S}_0 \leftarrow \text{Observe}(M, \mathbf{x}_0)$ 
5:    $\mathbf{x}_b \leftarrow \emptyset; \quad obj_b \leftarrow \infty$ 
6:   phase  $\leftarrow 1$ ; warmup  $\leftarrow \text{True}$ ; n_steps_grace  $\leftarrow 0$ 
7:   for  $t = 1, 2, \dots, T_{max}$  do
8:      $obj'_b \leftarrow obj_b$ 
9:      $\mathcal{A}_t \leftarrow \pi_\theta(\mathcal{S}_t)$ 
10:     $\mathcal{S}_{t+1}, \mathbf{x}_b, obj_b \leftarrow \text{Search}(\mathcal{S}_t, \mathcal{A}_t, \mathbf{x}_b, obj'_b, \text{phase})$  {See Algorithm 2}
11:     $\mathcal{R}_{t,\text{total}} \leftarrow \text{Reward}(M, \mathcal{S}_{t+1}, \mathcal{S}_t, obj_r, obj'_b, \text{phase})$  {See Equation 6}
12:     $\delta_{td} \leftarrow \mathcal{R}_{t,\text{total}} + \gamma \cdot V_\theta(\mathcal{S}_{t+1}) - V_\theta(\mathcal{S}_t)$ 
13:     $\mathcal{L}_\theta \leftarrow -\log \pi_\theta(\mathcal{A}_t | \mathcal{S}_t) \cdot \delta_{td} + \delta_{td}^2$ 
14:     $\theta \leftarrow \text{Update}(\mathcal{L}_\theta, \theta)$ 
15:    if phase = 1 and warmup = False then
16:      n_steps_grace  $\leftarrow$  n_steps_grace + 1
17:    else if phase = 2 then
18:      if  $\mathbf{x}_{t+1} \in \mathcal{F}$  then
19:        n_steps_grace  $\leftarrow 0$ 
20:      else
21:        n_steps_grace  $\leftarrow$  n_steps_grace + 1
22:      end if
23:    end if
24:    if warmup = True and  $t = T_{warm}$  then
25:      warmup  $\leftarrow$  False
26:       $\mathbf{x}_{t+1} \leftarrow \mathbf{x}_b$ 
27:    else if warmup = False and  $\mathbf{x}_{t+1} \in \mathcal{F}$  then
28:      phase  $\leftarrow 2$ 
29:      n_steps_grace  $\leftarrow 0$ 
30:    end if
31:    if n_steps_grace =  $T_{grace}$  or  $obj_r = obj_b$  then
32:      break
33:    end if
34:  end for
35: end for
36: return  $\theta$ 

```

D. Pseudo-Code for Solution Search Strategy

Our algorithm is designed to search for feasible solutions of a given instance M by exploring the neighborhood of the best solution found so far. The solution search process proceeds as follows: Based on \mathcal{A}_t , the next observation $\mathcal{S}_{t+1} = (\mathbf{x}_{t+1}, \mathbf{f}_{t+1}, obj_{t+1})$ are obtained (Line 1). If \mathbf{x}_{t+1} is feasible and obj_{t+1} is better (i.e., lower) than or equal to obj'_b , then obj_b and \mathbf{x}_b are updated to the new obj_{t+1} and \mathbf{x}_{t+1} , respectively (Lines 2-4). Updating \mathbf{x}_b implies that the center of the local region is also updated. The agent moves back to the center of the local region (i.e., \mathbf{x}_b) if it fails to find a better feasible solution and falls outside the local region in *phase1* (Lines 5-7). In *phase2*, the agent does not move unless it find a better feasible solution and moves back to the origin (Lines 8-10). The algorithm returns $\mathcal{S}_{t+1} = (\mathbf{x}_{t+1}, \mathbf{f}_{t+1}, obj_{t+1})$, \mathbf{x}_b , and obj_b (Line 12).

Algorithm 2 Solution Search Algorithm

Input: Observation $\mathcal{S}_t = (\mathbf{x}_t, \mathbf{f}_t, obj_t)$, Action \mathcal{A}_t , Best feasible solution \mathbf{x}_b , Best objective value obj'_b , Current phase *phase*

Parameter: Local region size Δ

Output: New observation \mathcal{S}_{t+1} , Best feasible solution \mathbf{x}_b , Best objective value obj_b

```

1:  $\mathcal{S}_{t+1} \leftarrow \text{Move}(\mathcal{S}_t, \mathcal{A}_t)$ 
2: if  $\mathbf{x}_{t+1} \in \mathcal{F}$  and  $obj_{t+1} \leq obj'_b$  then
3:    $obj_b \leftarrow obj_{t+1}$ 
4:    $\mathbf{x}_b \leftarrow \mathbf{x}_{t+1}$ 
5: else if phase = 1 and  $|x_{b,i} - x_{t+1,i}| > \Delta, \exists i$  then
6:    $obj_b \leftarrow obj'_b$ 
7:    $\mathbf{x}_{t+1} \leftarrow \mathbf{x}_b$ 
8: else if phase = 2 then
9:    $obj_b \leftarrow obj'_b$ 
10:   $\mathbf{x}_{t+1} \leftarrow \mathbf{x}_b$ 
11: end if
12: return  $\mathcal{S}_{t+1}, \mathbf{x}_b, obj_b$ 

```

E. Detail of Experimental Setup

E.1. Datasets Generation Process

Table 4 summarizes the parameters used for instance generation. Considering that the ratio of non-zero coefficients ρ in typical LP problems is less than 5% (Hillier & Lieberman, 2015), we set a higher density of 10% to promote more interactions between variables in constraints. According to the default settings of the SOTA optimizer Gurobi, the lower bound l_i and upper bound u_i for decision variables are set to 0 and ∞ , respectively. Training data is generated on-the-fly whenever the agent completes training on each instance, while test data is pre-generated in advance.

Table 4: Parameters for MILP instance generation.

Parameter	Distribution
c	$\text{randint}[-10, 1]$
A	$\text{randint}[1, 10]$ with density $\rho = 0.1$
b	$\mathbf{A}\xi + \epsilon$, where $\xi_i \sim \text{randint}[1, 10], \forall i = 1, \dots, n$ and $\epsilon_j \sim \text{randint}[1, 10], \forall j = 1, \dots, m$
I	$\{x \mid x \in \mathbb{N}, 1 \leq x \leq n\}$
l_i	$0, \forall i = 1, \dots, n$
u_i	$\infty, \forall i = 1, \dots, n$

E.2. Evaluation Environment

We conducted all evaluations under identical configurations. The evaluation machine is equipped with two Intel Xeon Silver 4214R CPUs @ 2.4GHz, 768GB RAM, and eight NVIDIA Titan RTX GPUs. All experiments were performed using a single NVIDIA Titan RTX GPU. The software environment includes PyTorch 1.10.2, Gymnasium 0.29.1, and Gurobi 9.5.2.

E.3. Method Implementation

We utilize the bipartite graph convolution available on GitHub¹ (Han et al., 2023), as the architecture for our MPNN. Two iterations of the process shown in Figure 2(a) are applied, resulting in two constraint-side and two variable-side convolutions. Our proposed model is implemented using the Transformer encoder code from GitHub² (Wu et al., 2021), maintaining the same configuration. We developed two MPNN-based baselines, M_MLP and M_CNN. M_MLP consists of four MLP layers with a hidden size of 128 and tanh activation, while M_CNN includes four CNN layers followed by an MLP layer with ReLU activation. We utilized the positional encoding module from GitHub³ (Gorishniy et al., 2022).

All ML models were trained using the proposed learning algorithm (Algorithm 1) with RMSprop (learning rate = $1e-4$, epsilon = $1e-5$, alpha = 0.99, weight decay = $1e-3$). They were trained concurrently on 64 different instances with 5,000 parameter updates for the results in Tables 1 and 3, and 10,000 for Table 2. Our RL algorithm is built upon the Actor-Critic implementation in PyTorch⁴ (Kostrikov, 2018), modified to be tailored for MILP problems.

¹https://github.com/sribdcn/Predict-and-Search_MILP_method

²<https://github.com/ucbrise/graphtrans>

³<https://github.com/yandex-research/rtdl-num-embeddings>

⁴<https://github.com/ikostrikov/pytorch-a2c-ppo-acktr-gail>